Electrochemical Sodium Ion Intercalation Properties of $Na_{2.7}Ru_4O_9$ in Nonaqueous and Aqueous Electrolytes

Journal of The Electrochemical Society, **160** (6) A897-A900 (2013)
0013-4651/2013/160(6)/A897/4/$31.00 © The Electrochemical Society

Electrochemical Sodium Ion Intercalation Properties of $Na_{2.7}Ru_4O_9$ in Nonaqueous and Aqueous Electrolytes

Young Hwa Jung,[a] Seung-Tae Hong,[b,z] and Do Kyung Kim[a,z]

[a]*Department of Materials Science and Engineering, KAIST, Daejeon 305-701, Korea*
[b]*Department of Energy Systems Engineering, DGIST, Daegu 711-873, Korea*

This paper represents the first description of the electrochemical sodium ion intercalation properties of $Na_{2.7}Ru_4O_9$ in both nonaqueous and aqueous electrolytes. $Na_{2.7}Ru_4O_9$ was synthesized at 700–850°C by solid-state reaction under Ar flow. It has single, double and triple chains of edge-sharing RuO_6 octahedra and one-dimensional tunnels between them parallel to the *b*-axis, accommodating three different sites of Na1, Na2 and Na3. In an organic electrolyte (1 M $NaClO_4$ in PC), $Na_{2.7}Ru_4O_9$ shows three redox peaks in its cyclic voltammogram between 2.8 and 3.9 V vs. Na. In an aqueous (1 M Na_2SO_4) electrolyte, $Na_{2.7}Ru_4O_9$ exhibits three anodic peaks during the first charge, similar to the behavior observed in the organic electrolyte. However, the three peaks become a single broad peak over the following cycles. Electrochemical data and ex-situ XRD results indicate that once Na ions are removed from the $Na_{2.7}Ru_4O_9$ structure containing the maximum amount of sodium, only a portion (<60%) can be re-intercalated and that the aqueous electrolyte allows a lower reversible capacity than the nonaqueous electrolyte.
 [DOI: 10.1149/2.113306jes]

Manuscript submitted January 28, 2013; revised manuscript received March 8, 2013. Published April 10, 2013. This was Paper 1864 presented at the Honolulu, Hawaii, Meeting of the Society, October 7–12, 2012.

The development of rechargeable lithium-ion batteries (LIBs) for mobile electronic devices, electric vehicles and energy storage systems has made tremendous progress since lithium intercalation electrode materials have been heavily investigated over the past several decades.[1–3] Although Li-based rechargeable batteries are currently the dominant battery type, concerns about high cost and safety of lithium batteries have been significantly increasing.[4–6] To overcome these drawbacks of LIBs, studies on Na-based materials have been receiving increasing attention due to the abundance and low cost of sodium.[7–9] Many of the crystal structures are common to both Li and Na electrode materials. It is, however, not always straightforward to find or predict whether a structure is sufficiently stable or electrochemically active for the intercalation of sodium ions. A typical example is maricite, $NaFePO_4$: its thermodynamically more stable form at high temperature is electrochemically inactive, in contrast to its olivine form.[10,11] In that sense, finding a novel Na intercalation material with a distinctive crystal structure can contribute to the improvement of Na-based rechargeable batteries.

Among various intercalation host materials for rocking-chair batteries, one-dimensional (1-*d*) tunnel structures have received attention by providing stable framework for host ions. While 1-*d* tunnel structures as lithium ion intercalation materials are intensively investigated,[12–14] sodium intercalation materials with 1-*d* tunnel structures are rarely studied.[15,16] In our previous work,[15] we verified the structural and electrochemical properties of $Na_{0.44}MnO_2$, a sodium intercalation host material with a 1-*d* tunnel structure. $Na_{0.44}MnO_2$ showed five biphasic transitions;[16] however, we found that seven intermediate phases arise from electrochemical reactions that occur in the range of 0.22 to 0.66 Na by density functional theory calculations. In addition, it was found that the S-shaped tunnel is not empty in the deintercalated $Na_{0.22}MnO_2$ structure but is partially occupied by sodium ions.

In view of the aforementioned part, this study was motivated by the search for other structures similar to $Na_{0.44}MnO_2$ to understand and verify the electrochemical Na insertion properties of such 1-*d* tunnel structures. Here, we introduce a new sodium ion intercalation material, $Na_{2.7}Ru_4O_9$, with a similar 1-*d* tunnel structure to, but different polyhedral networks from, that of $Na_{0.44}MnO_2$. The crystal structure and nonstoichiometric composition of $Na_{3-x}Ru_4O_9$ was first reported by Darriet,[17] and later, the more precise stoichiometry was determined to be $x = 0.3$ by Regan et al.[18] $Na_{2.7}Ru_4O_9$, isostructural with $Na_2Ti_4O_9$ in a monoclinic lattice (space group *C*2/*m*, No.12), has 1-*d* tunnels parallel to the *b*-axis with single, double and triple chains of edge-sharing RuO_6 octahedra, which can accommodate three different sites of Na1, Na2 and Na3, as shown in Fig. 1. Na3, placed between Na1 and Na2, is coordinated with 6 oxygen atoms, while Na1 and Na2 are 8-coordinated. We describe the electrochemical sodium ion intercalation properties of $Na_{2.7}Ru_4O_9$ in both nonaqueous and aqueous solutions.

Experimental

$Na_{2.7}Ru_4O_9$ was synthesized via a solid-state route from a mixture of Na_2CO_3 (99.5%, Aldrich) and RuO_2 (99.9%, Aldrich) with a nominal composition of Na : Ru = 1.42 : 2. A 5 wt% excess of Na_2CO_3 was added to compensate for the evaporation of sodium during the synthesis. The reaction mixtures were ground in an agate mortar, pressed

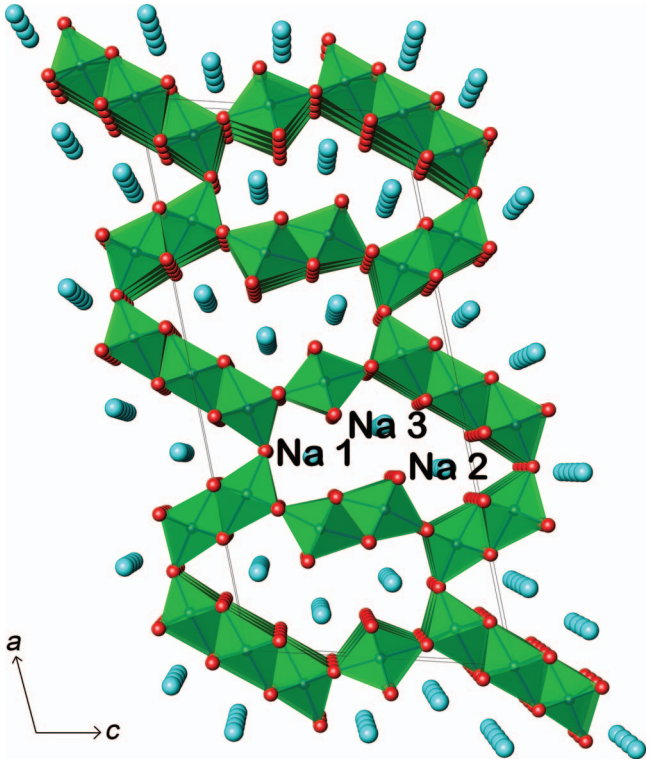

Figure 1. Crystal structure of $Na_{2.7}Ru_4O_9$ perpendicular to the *ac* plane.

[z]E-mail: st.hong@dgist.ac.kr; dkkim@kaist.ac.kr

into 10 mm diameter pellets, and heated at 700°C for 12 h and 850°C for 6 h under argon flow.

Powder X-ray diffraction (XRD) data were collected at room temperature on a Bragg-Brentano diffractometer (Bruker Advance D8) with a Cu X-ray tube, a focusing primary Ge (111) monochromator ($\lambda = 1.5405$ Å) and a position-sensitive Väntec detector with a 6° slit. The acquired data covered the angular range of $8° \leq 2\theta \leq 140°$ at a step width of 0.01668°. The crystal structure of $Na_{2.7}Ru_4O_9$ was confirmed and refined using the powder profile refinement program GSAS.[19] Ex-situ XRD measurements were carried out using a PANalytical Empyrean X-ray diffractometer with a Cu X-ray tube ($\lambda = 1.5418$ Å) and a position-sensitive PIXcell detector at room temperature. The morphology of the synthesized particles was characterized using scanning electron microscopy (FE-SEM, Philips, XL-30).

The electrodes used for electrochemical testing were fabricated by combining $Na_{2.7}Ru_4O_9$, carbon black and PVdF binder in a weight ratio of 80:10:10 on stainless steel foils. The loading of the active material was approximately $1 \sim 2$ mg/cm^2. Beaker-type cells were assembled to characterize the performance of the $Na_{2.7}Ru_4O_9$ electrodes using Na metal as the counter and reference electrodes in an Ar-filled glove box ($[H_2O]$ and $[O_2] < 1$ ppm). The electrolyte was 1 M $NaClO_4$ in propylene carbonate. Three-electrode electrochemical cells were assembled to test the electrodes in an aqueous electrolyte. A saturated calomel electrode (SCE), a large piece of sodium-extracted $Na_{0.44-x}MnO_2$ coated on a stainless steel foil and a 1 M Na_2SO_4 aqueous solution were used as the reference electrode, counter electrode and electrolyte, respectively.[20,21] Cyclic voltammetry and galvanostatic charge/discharge tests were performed using a VMP3 potentiostat (Bio-Logic). All measurements were conducted at ambient temperature.

Results and Discussion

The refined crystal structure is presented in Fig. 1, where RuO_6 and Na ions are shown as octahedra and spheres, respectively. Fig. 2 shows the Rietveld refinement profile for a $Na_{2.7}Ru_4O_9$ powder. The important refined parameters are the lattice constants, preferred orientation (010 and 100 direction), atom positions, and Na occupancies, starting from the previously reported monoclinic structure ($C2/m$),[18] and the refined lattice parameters are $a = 23.3491(6)$ Å, $b = 2.8300(3)$ Å, $c = 11.0089(4)$ Å, $\beta = 104.628(3)°$ and $V = 703.88(8)$ Å^3. A small amount ($< 2\%$) of impurity phase was also observed and identified as $NaRu_2O_4$. The corresponding peaks are indicated by the red ticks. The SEM image (inset of Fig. 2) shows that the crystals grow as long needles measuring tens of micrometers in length, presumably along the shortest *b*-axis, which conforms to the refined preferred orientation (P.O.) coefficients in the Rietveld refinement: the March-Dollase type P.O. coefficients of [1 0 0] and [0 1 0] are 0.54 and 1.74 with the fraction of 6% and 94%, respectively. Although all three Na sites can be partially occupied, as initially reported by Darriet,[17] our Rietveld refinement suggests that only the Na3 site has a partial occupancy of 0.7, consistent with the previous results.[18] As expected from its crystal structure, the main path for sodium ion diffusion is parallel to the *b* direction, and the neighboring Na-Na distance is approximately 2.83 Å, the *b*–axis length.

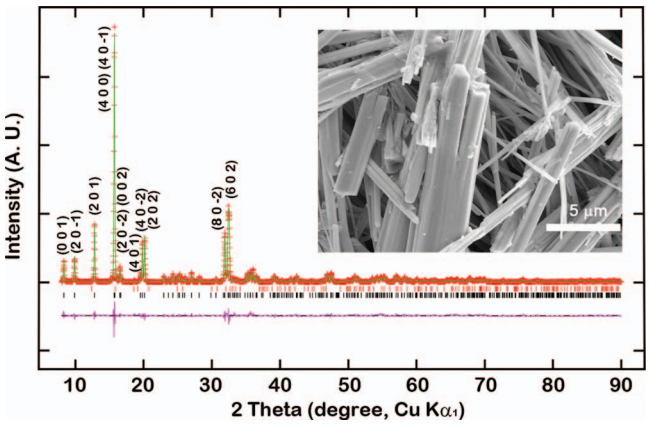

Figure 2. X-ray Rietveld refinement profiles for $Na_{2.7}Ru_4O_9$ powders, including the minor impurity of $NaRu_2O_4$, recorded at room temperature. The cross lines mark the experimental points (red), and the solid lines are the calculated profiles (green). The bottom traces show the difference curve (purple), and the ticks denote the expected peak positions for $Na_{2.7}Ru_4O_9$ (black) and $NaRu_2O_4$ (red). The inset shows an SEM image of $Na_{2.7}Ru_4O_9$ particles obtained by solid-state reaction.

$Na_{2.7}Ru_4O_9$ was electrochemically characterized in an organic electrolyte using Na metal half-cells in an Ar-filled glove box. The $Na_{2.7}Ru_4O_9$/Na half-cell shows an initial open circuit potential of approximately 2.8 V vs. Na/Na$^+$. Fig. 3a shows the first cyclic voltammogram of $Na_{2.7}Ru_4O_9$ at a scan rate of 0.05 mV s^{-1} between 2.8 and 3.9 V vs. Na in a 1 M $NaClO_4$/PC electrolyte. It exhibits three anodic peaks (sodium desertion) at 3.22, 3.66 and 3.73 V, and the three corresponding peaks (sodium insertion) at 3.13, 3.54 and 3.69 V, respectively, demonstrate the reversible electrochemical sodium intercalation reaction in $Na_{2.7}Ru_4O_9$. The potential vs. composition (x) profile of $Na_xRu_4O_9$ obtained from a galvanostatic experiment performed at a C-rate of 1/15 (1 C = 119 mA g^{-1}, corresponding to all Na extracted) is shown in Fig. 3b. When charged from its initial composition of $Na_{2.7}Ru_4O_9$ to 3.8 V, the material delivers a capacity of 83 mAh g^{-1}, corresponding to the removal of about 1.9 moles of Na per mole of Ru_4O_9, ~70% of the full 2.7 moles of Na. To remove the Na ions completely from $Na_{2.7}Ru_4O_9$, charging up to a potential much higher than 3.8 V would be necessary, though it was not able to be confirmed experimentally because the electrolyte decomposition would also occur simultaneously at such a potential. It is also anticipated that the complete removal of Na ions from the tunnel structure would make the structure unstable, as observed in $Na_{0.44}MnO_2$.[13] The first discharge capacity delivers approximately 49 mAh g^{-1} with a coulombic efficiency of ~59%, demonstrating a low reversibility in this structure: only ~1.1 Na$^+$ ions are inserted back into the structure. It seems that the maximum amount of Na ions, 2.7 moles per a formula Ru_4O_9, can only be obtained thermodynamically when synthesized at high temperature. Once the Na ions are removed from the structure, it is difficult to fully re-insert the ions back into the large tunnels electrochemically at room temperature, probably because of the strong Na-Na repulsion in the crowded tunnels due to the large ionic size of Na; a similar reason for why the Na3 site cannot be fully occupied was reported by Regan et al.[18]

The rate characteristics of a $Na_{2.7}Ru_4O_9$ electrode galvanostatically cycled in the voltage range of 2.8 to 3.9 V are shown in Fig. 3c. The discharge capacity at 1 C was reduced to approximately 30% of that at 0.1 C, indicating the slow diffusion of Na ions, as observed in other Na-based electrode materials.[22–24] Large micro-sized particles may be an additional cause for the low rate capability, which is known to be an obstacle to fast ionic diffusion in one-dimensional structures.[25]

To compare the electrochemical properties of $Na_{2.7}Ru_4O_9$ in an organic electrolyte with those of $Na_{2.7}Ru_4O_9$ in an aqueous electrolyte, the cyclic voltammogram of $Na_{2.7}Ru_4O_9$ was also measured in a 1 M Na_2SO_4 aqueous electrolyte using three-electrode cells (Fig. 4a). The extraction of Na ions corresponds to the three anodic peaks at 0.31, 0.69 and 0.73 V vs. SCE during the first oxidation step, which are equivalent to 3.28, 3.66 and 3.70 V vs. Na, respectively, considering an SCE voltage of 2.97 V vs. Na. These peaks match very well with those observed in the organic electrolyte. During the next reduction process and the following cycles, however, the intercalation reaction in the aqueous medium looks significantly different from that in the organic electrolyte. Only one broad cathodic and one anodic peak are observed at approximately 0.42 V and 0.53 V vs. SCE (corresponding to ~3.4 V and ~3.5 V vs. Na), respectively. The galvanostatic charge/discharge measurements (Fig. 4b) also show results that are consistent with the

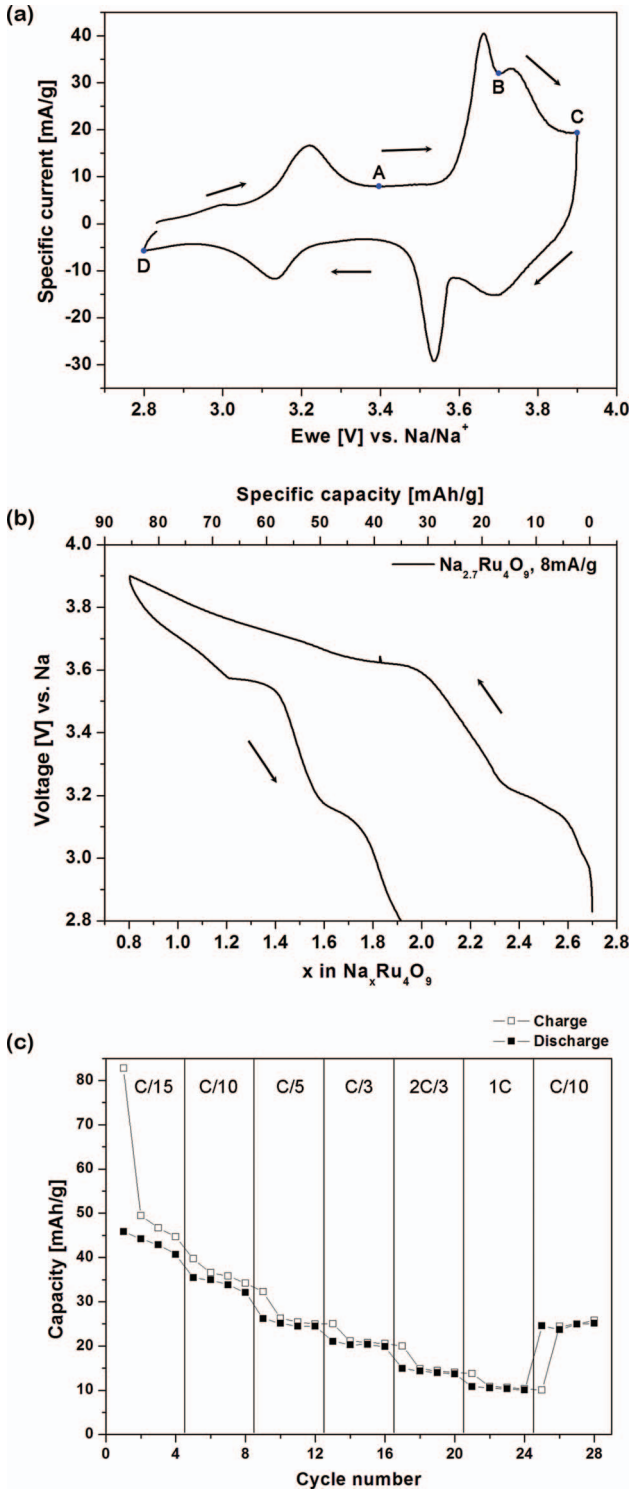

Figure 3. (a) Cyclic voltammogram of $Na_{2.7}Ru_4O_9$ in 1 M $NaClO_4$/PC electrolyte at a scan rate of 0.05 mV s^{-1} between 2.8 and 3.9 V. (b) Voltage vs. composition profile of $Na_{2.7}Ru_4O_9$ obtained from galvanostatic charge/discharge at a current of 8 mA g^{-1} between 3.9 and 2.8 V. (c) Charge and discharge capacity of $Na_{2.7}Ru_4O_9$ at different current rates.

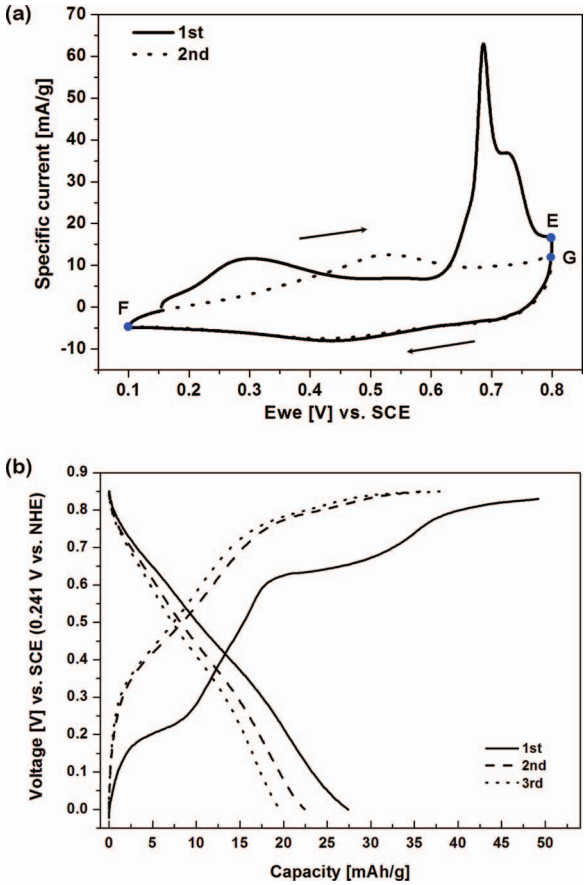

Figure 4. (a) A cyclic voltammogram of $Na_{2.7}Ru_4O_9$ collected from a three-electrode cell in a 1 M Na_2SO_4 electrolyte at a scan rate of 0.05 mV s^{-1} between 0.1 and 0.8 V vs. SCE reference electrode. (b) Galvanostatic charge and discharge profiles of $Na_{2.7}Ru_4O_9$ at a current rate of 3 mA g^{-1} in a 1 M Na_2SO_4 electrolyte.

cyclic voltammograms. Three plateaus are clearly evident during the first oxidation process but disappear in the following cycling process, leaving a simpler sloping profile.

To investigate the structural changes that occur during electrochemical intercalation, ex-situ X-ray diffraction studies were performed. In each of the steps, the electrode was held under the test conditions for more than 3 hours to reach equilibrium. Fig. 5 compares the XRD patterns of the charged and discharged electrodes after the electrochemical tests in the nonaqueous and aqueous electrolytes. It is apparent that the main crystal structure is retained during the electrochemical reaction. In nonaqueous systems (Fig. 5a), A, B, and C refer to the electrodes initially charged up to 3.4 V, 3.7 V, and 3.9 V, respectively, and D refers to the electrode fully discharged down to 2.8 V; the points are as denoted in Fig. 3a. Most of peak positions are preserved after the first oxidation peak at point A and slightly shifted after the second oxidation peak at point B. Further oxidation at point C results in the considerable shift in all peaks. As clearly observed from the (0 0 1) and (4 0 0) peaks, the cell parameter *a* increases, while *c* decreases as Na is extracted. When the Na ions are re-inserted (discharged to point D), the peak positions and intensity ratio are restored, though not completely, to those in the initial state at point A. This is consistent with the results of the galvanostatic experiments (Fig. 3b), which indicate that only 70% (1.9 out of 2.7) of Na ions are re-inserted into the structure after discharge. Although we are not able to precisely verify which particular Na site is responsible for each step of the de/insertion processes, we presume that all three Na sites are involved, interactively affecting the electrochemical reaction in this material, as observed in $Na_{0.44}MnO_2$.[15]

The XRD patterns obtained after running the electrochemical reactions in aqueous systems are presented in Fig. 5b. The patterns for the charged states in the aqueous (E) and organic electrolytes (C) are similar to each other in terms of major peak shifts. A noticeable difference between the two electrolytes is that the discharged pattern (F)

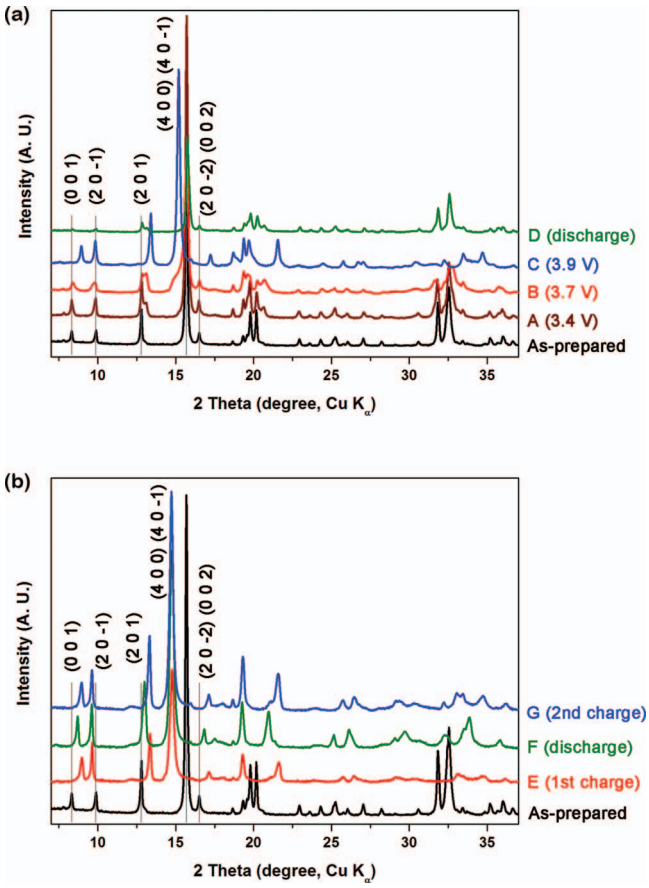

Figure 5. Ex situ X-ray diffraction patterns of $Na_{2.7}Ru_4O_9$ in the charged and discharged state during the first cycle in (a) an organic electrolyte of 1 M $NaClO_4$/PC and (b) aqueous electrolyte of 1 M Na_2SO_4.

shows a slight change from the charged one (E and G) in the aqueous electrolyte, not returning to the original peak positions at all. After re-charging it in the second cycle (point G), the XRD pattern looks almost the same as the pattern obtained after the first charge. These results show that once the Na ions are extracted from the structure in the aqueous electrolyte, only a small amount of Na ions (less than 30 mAh g^{-1}) are re-inserted compared to the amount re-inserted in the structure in the nonaqueous electrolyte. The reason for this difference is not clear, but it could be related to the solvation effect of water on the surface of the electrode. In rechargeable aqueous lithium ion batteries, several problems have already been reported such as the reaction between electrode materials and water or O_2, proton co-intercalation, side reactions in aqueous electrolytes, and the dissolution of electrode materials.[26] The sodium insertion materials in aqueous media may show similar behaviors as the lithium systems. Our future study will focus on deep understanding the phenomena of electrochemical sodium insertion into crystal structures in aqueous electrolytes.

Conclusions

$Na_{2.7}Ru_4O_9$ was synthesized by a solid-state reaction, and the electrochemical properties of Na intercalation were examined as a new sodium intercalation host material with a one-dimensional tunnel structure. The unique network structure of RuO_6 octahedra provides one-dimensional chains that are large enough to accommodate three Na sites. In a nonaqueous electrolyte, the material shows three peaks in its CV or three plateaus in its galvanostatic charge/discharge curve between 2.8–3.9 V vs. Na, indicating the presence of multiple biphasic and single-phase domains in the structure during the Na intercalation reaction. The initial charge capacity of $Na_{2.7}Ru_4O_9$ is ~ 83 mAh g^{-1}, whereas the following discharge capacity is only ~ 49 mAh g^{-1}. In the aqueous electrolyte, the first charge appears to be very similar to that observed in the organic electrolyte. However, once the electrode is initially charged, the following Na insertion/desertion processes exhibit only one broad peak in the CV or a sloppy profile in the discharge/charge curve with a much lower discharge capacity (~27 mAh g^{-1} or less). Ex-situ XRD results reveal that the $Na_{2.7}Ru_4O_9$ structure itself seems to be maintained during the intercalation reaction, showing expansion or contraction of the lattice. The degree of change in the lattice constants conforms to the observed amount of Na removed or inserted. To the best of our knowledge, this study represents the first time that the electrochemical sodium intercalation of $Na_{2.7}Ru_4O_9$-type compound has been characterized. Further work will be necessary to fully understand the intercalation chemistry of the structure. This work could provide an important basis for understanding the structure-property correlation in the sodium ion intercalation chemistry of new materials.

Acknowledgments

This work was supported by the Program to Solve Climate Changes (NRF-2010-C1AAA001-2010-0029031) through the National Research Foundation of Korea (NRF) funded by the Ministry of Education, Science and Technology. It was also supported by the DGIST R&D Program of the Ministry of Education, Science and Technology of Korea (13-BD-0403).

References

1. M. Armand and J.-M. Tarascon, *Nature*, **451**, 652 (2008).
2. Z. Yang, J. Zhang, M. C. W. Kintner-Meyer, X. Lu, D. Choi, J. P. Lemmon, and J. Liu, *Chem. Rev.*, **111**, 3577 (2011).
3. T.-H. Kim, J.-S. Park, S. K. Chang, S. Choi, J. H. Ryu, and H.-K. Song, *Adv. Energy Mater.*, **2**, 860 (2012).
4. J.-M. Tarascon, *Nat. Chem.*, **2**, 510 (2010).
5. J. B. Goodenough and Y. Kim, *J. Power Sources*, **196**, 6688 (2011).
6. Z. Yang, J. Zhang, M. C. W. Kintner-Meyer, X. Lu, D. Choi, J. P. Lemmon, and J. Liu, *Chem. Rev.*, **111**, 3577 (2011).
7. S.-W. Kim, D.-H. Seo, X. Ma, G. Ceder, and K. Kang, *Adv. Energy Mater.*, **2**, 710 (2012).
8. V. Palomares, P. Serras, I. Villaluenga, K. B. Hueso, J. C-Gonzalez, and T. Rojo, *Energy Environ. Sci.*, **5**, 5884 (2012).
9. B. L. Ellis and L. F. Nazar, *Curr. Opin. Solid State Mat. Sci.*, **16**, 168 (2012).
10. B. L. Ellis, W. R. M. Makahnouk, Y. Makimura, K. Toghill, and L. F. Nazar, *Nat. Mater.*, **6**, 749 (2007).
11. S. P. Ong, V. L. Chevrier, G. Hautier, A. Jain, C. Moore, S. Kim, X. Ma, and G. Ceder, *Energy Environ. Sci.*, **4**, 3680 (2011).
12. C. S. Johnson and M. M. Thackeray, *J. Power Sources*, **97–98**, 437 (2001).
13. J. A. Saint, M. M. Doeff, and J. Wilcox, *Chem. Mater.*, **20**, 3404 (2008).
14. L.-X. Yuan, Z.-H. Wang, W.-X. Zhang, X.-L. Hu, J.-T. Chen, Y.-H. Huang, and J. B. Goodenough, *Energy Environ. Sci.*, **4**, 269 (2011).
15. H. Kim, D. Kim, D. Seo, M. Yeom, K. Kang, D. Kim, and Y. Jung, *Chem. Mater.*, **24**, 1205 (2012).
16. F. Sauvage, L. Laffont, J.-M. Tarascon, and E. Baudrin, *Inorg. Chem.*, **46**, 3289 (2007).
17. J. Darriet, *Acta Cryst. B*, **30**, 1459 (1974).
18. K. A. Regan, Q. Huang, M. Lee, A. P. Ramirez, and R. J. Cava, *J. Solid State Chem.*, **179**, 195 (2006).
19. A. C. Larson and R. B. Von Dreele, GSAS; Report LAUR 86-748 (2000) Los Alamos National Laboratory, New Mexico, USA.
20. R. Ruffo, C. Wessells, R. A. Huggins, and Y. Cui, *Electrochem. Comm.*, **11**, 247 (2009).
21. J. F. Whitacre, A. Tevar, and S. Sharma, *Electrochem. Comm.*, **12**, 463 (2010).
22. M. D'Arienzo, R. Ruffo, R. Scotti, F. Morazzoni, C. M. Mari, and S. Polizzi, *Phys. Chem. Chem. Phys.*, **14**, 5945 (2012).
23. Y. Cao, L. Xiao, W. Wang, D. Choi, Z. Nie, J. Yu, L. V. Saraf, Z. Yang, and J. Liu, *Adv. Mater.*, **23**, 3155 (2011).
24. Z. Jian, L. Zhao, H. Pan, Y.-S. Hu, H. Li, W. Chen, and L. Chen, *Electrochem. Comm.*, **14**, 86 (2012).
25. R. Malik, D. Burch, M. Bazant, and G. Ceder, *Nano Lett.*, **10**, 4123 (2010).
26. Y. Wang, J. Yi, and Y. Xia, *Adv. Energy Mater.*, **2**, 830 (2012).